iScience

Article

The role of the tricellular junction protein ILDR2 in glomerulopathies: Expression patterns and functional insights

Graphical abstract

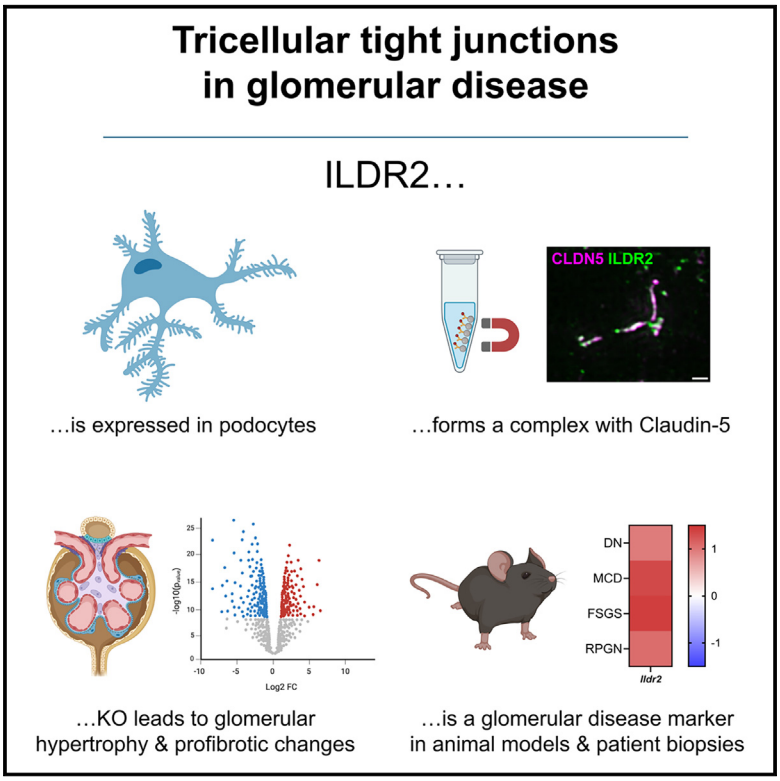

Highlights

- ILDR2 is expressed in podocytes and builds a complex with the podocyte-specific claudin-5
- Due to its uniform upregulation, ILDR2 can serve as a glomerular disease marker
- *Ildr2* knockout mice exhibited glomerular hypertrophy and decreased podocyte density
- Glomeruli of *Ildr2* KO mice showed an increase in matrix proteins

Authors

Florian Siegerist, Felix Kliewe, Elke Hammer, ..., Matthias Nauck, Uwe Völker, Nicole Endlich

Correspondence

nicole.endlich@uni-greifswald.de

In brief

Natural sciences; Biological sciences; Physiology; Cellular physiology

Siegerist et al., 2024, iScience 27, 111329
December 20, 2024
https://doi.org/10.1016/j.isci.2024.111329

CellPress

iScience

CellPress
OPEN ACCESS

Article

The role of the tricellular junction protein ILDR2 in glomerulopathies: Expression patterns and functional insights

Florian Siegerist,[1,12] Felix Kliewe,[1] Elke Hammer,[2] Paul Schakau,[1] Joanne Ern Chi Soh,[1] Claudia Weber,[1] Maja Lindenmeyer,[3,4] Simone Reichelt-Wurm,[5] Vedran Drenic,[6] Christos Chatziantoniou,[7] Christos E. Chadjichristos,[7] Yiying Zhang,[8] Stefan Simm,[9,10] Miriam C. Banas,[5] Matthias Nauck,[11] Uwe Völker,[2] and Nicole Endlich[1,6,13,*]

[1]Department of Anatomy and Cell Biology, University Medicine Greifswald, Greifswald, Germany
[2]Interfaculty Institute for Genetics and Functional Genomics, University Medicine Greifswald, Greifswald, Germany
[3]III. Department of Medicine, University Medical Center Hamburg-Eppendorf, Hamburg, Germany
[4]Hamburg Center for Kidney Health (HCKH), University Medical Center Hamburg-Eppendorf, Hamburg, Germany
[5]Department of Nephrology, University Hospital Regensburg, Regensburg, Germany
[6]NIPOKA GmbH, Center of High-End Imaging, Greifswald, Germany
[7]National Institute for Health and Medical Research (INSERM), Unité Mixte de Recherche (UMR)-S1155, Tenon Hospital, Sorbonne Universités, Paris, France
[8]Vagelos College of Physicians and Surgeons, Medical School of Columbia University, New York, NY, USA
[9]Institute of Bioinformatics, University Medicine Greifswald, Greifswald, Germany
[10]Institute of Bioanalysis, Coburg University of Applied Sciences, Coburg, Germany
[11]Institute for Clinical Chemistry and Laboratory Medicine, University Medicine, Greifswald, Germany
[12]Present address: Department for Pediatrics, University Medicine Greifswald, Greifswald, Germany
[13]Lead contact
*Correspondence: nicole.endlich@uni-greifswald.de
https://doi.org/10.1016/j.isci.2024.111329

SUMMARY

The tricellular tight junctions are crucial for the regulation of paracellular flux at tricellular junctions, where tricellulin (MARVELD2) and angulins (ILDR1, ILDR2, or LSR) are localized. The role of ILDR2 in podocytes, specialized epithelial cells in the kidney, is still unknown. We investigated the role of ILDR2 in glomeruli and its influence on blood filtration. Western blots, single-cell RNA sequencing (scRNA-seq), and superresolution microscopy showed a strong expression of ILDR2 in podocytes that colocalized with the podocyte-specific claudin CLDN5. Co-immunoprecipitation revealed that ILDR2 interacts with CLDN5. In glomerulopathies, induced by nephrotoxic serum and by desoxycorticosterone acetate (DOCA)-salt heminephrectomy, ILDR2 was strongly up-regulated. Furthermore, *Ildr2* knockout mice exhibited glomerular hypertrophy and decreased podocyte density. However, they did not develop effacement of podocyte foot processes or proteinuria. Liquid chromatography-tandem mass spectrometry (LC-MS/MS) proteomic analysis of isolated glomeruli showed an increase in matrix proteins, such as fibronectin and collagens. This suggests a protective role of ILDR2 in glomerulopathies.

INTRODUCTION

Podocytes, a terminally differentiated cell type in the glomeruli, are essential for maintaining the integrity of the glomerular filtration barrier. These cells, characterized by interdigitating foot processes with filtration slits in between, are critical for the size selectivity of the filtration barrier, a property that is crucial for renal filtration function. Previous studies have shown that the slit diaphragm can also be considered as a specialized adherens and tight junction, as it not only expresses a combination of characteristic slit diaphragm proteins, such as nephrin and podocin, but also tight junction proteins such as ZO-1.[1] Although podocyte junctions exist predominantly as bicellular connections, tricellular contacts have also been described, as shown by detailed reconstructions using scanning electron microscopy (SEM).[2]

At sites of tricellular tight junctions (tTJs), specific proteins, such as tricellulin MARVELD2 (MARVEL domain-containing protein 2) and proteins of the angulin family such as LSR (lipolysis-stimulated lipoprotein receptor), ILDR1 or ILDR2 (immunoglobulin-like domain-containing receptor 1/2) are expressed.[3] tTJs further influence the barrier function of epithelial and endothelial tissues, allowing the paracellular transport, e.g., of molecules and ions[4] even independently of claudins.[5] It was reported that they could also play a mechanosensory role[6] and is able to recruit claudins to the tTJs.[3] Over decades, studies have shown that mutations in tTJ components are linked to a variety of diseases.[5] Loss of tTJs components that govern

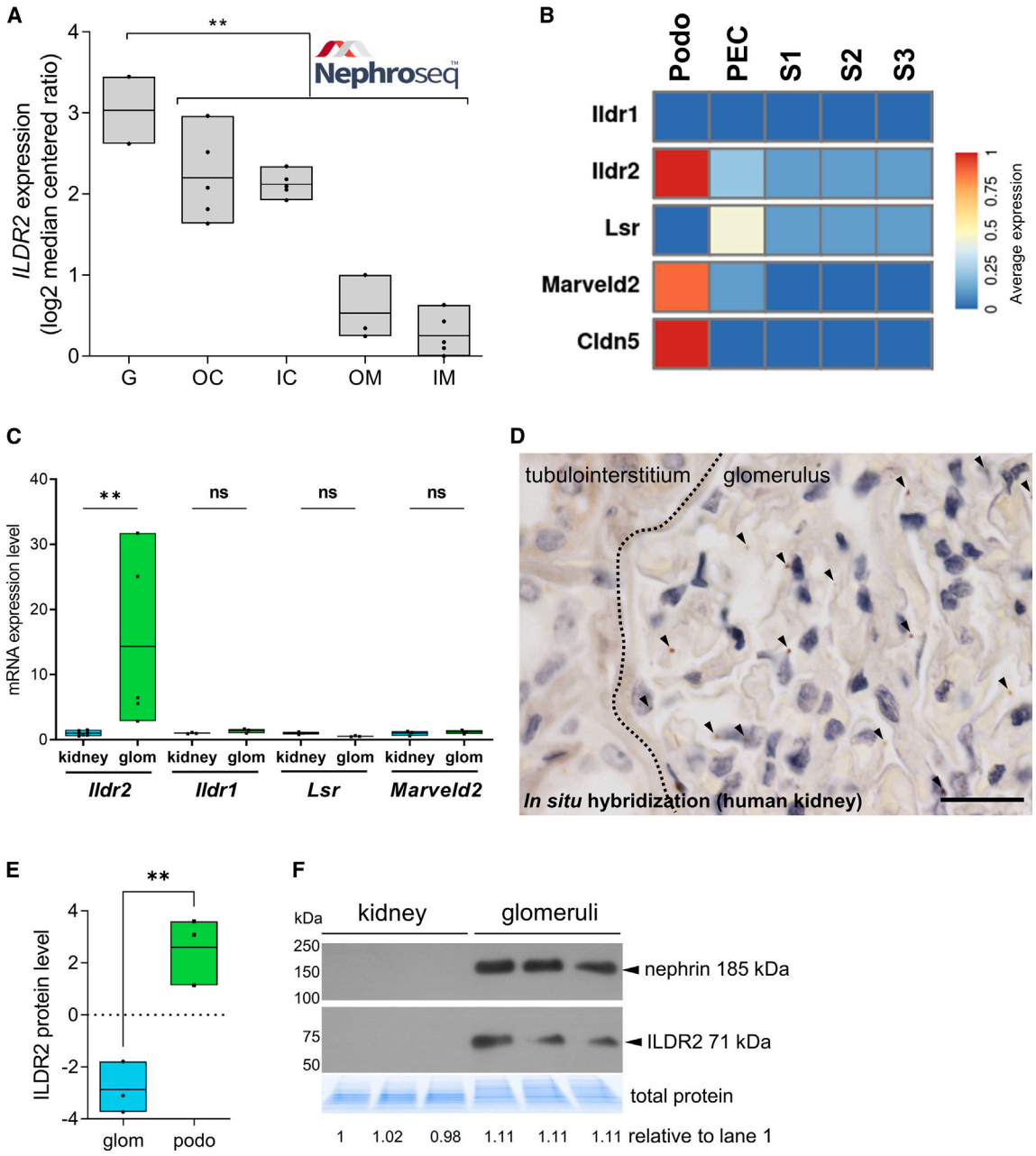

Figure 1. *ILDR2* expression in human and mouse kidney tissue

(A) *ILDR2* expression in glomeruli (G), outer renal cortex (OC), inner renal cortex (IC), outer renal medulla (OM), and inner renal medulla (IM). Data are represented as log2 median centered ratio. Each dot represents one sample. Data were taken from www.nephroseq.org.

(B) Database analysis of *Ildr2* in podos (podocytes), PECs (parietal epithelial cells), and PT (segment 1, 2, or 3 of proximal tubule) using the KidneyCellExplorer (Ransick et al., 2019) based on a single-cell RNA sequencing dataset of murine kidneys.[9]

(C) The mRNA expression of *Ildr2*, *Ildr1*, *Lsr*, and *Marveld2* in isolated glomeruli and murine kidneys was quantified by RT-qPCR ($n \geq 3$). RT-qPCR experiments were normalized to the kidney samples and *Gapdh*.

(D) *In situ* hybridization of *ILDR2* in human kidney tissue. ILDR2-positive mRNA spots are marked by arrowheads. Nuclei are shown in blue. Scale bar represents 20 μm.

(E) Podocyte proteome data (Rinschen et al.[10]) showed an enrichment of ILDR2 protein level in podocytes compared to glomeruli.

(F) Western blot confirmed glomerulus-specific expression of ILDR2 ($n = 3$). Nephrin served as positive control and total protein (visualized by Stain-Free technology) served as a loading control. $^{**}p < 0.01$. Data are presented as floating bars (A, C, and E).

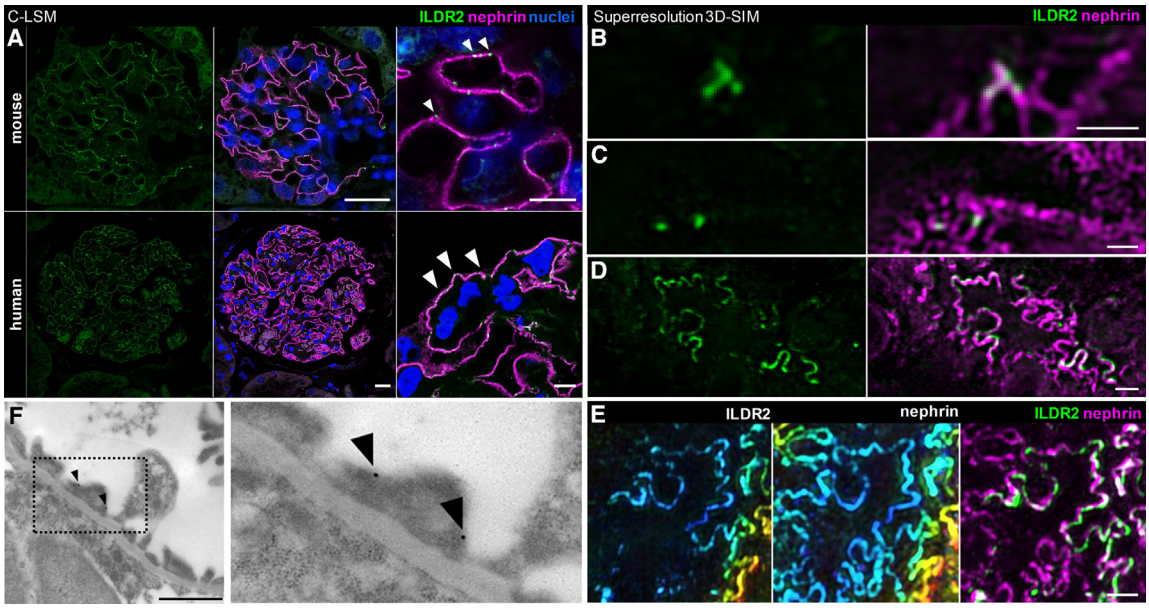

Figure 2. Podocytes express the tricellular tight junction-associated protein ILDR2

(A) Immunofluorescence staining for ILDR2 (green) and the podocyte-specific marker nephrin (magenta) in mouse and human kidney tissue. Nuclei were stained with Hoechst (blue). Scale bars represent 20 μm and 5 μm (magnification), respectively.

(B and C) Super-resolution 3D-structured illumination microscopy (3D-SIM) revealed that ILDR2 (shown in green) localized to tricellular junctions as indicated by a co-staining with nephrin (shown in magenta) on Y-intersections of the nephrin-stained filtration slit and to bicellular junctions in a spotted manner within healthy-appearing foot processes.

(D and E) Immunofluorescence staining of kidney sections of E19 embryonic mouse kidneys (D) and adult mouse kidneys (E) showed that ILDR2 broadly localized to effaced podocyte filtration slits as indicated by a linearized double ILDR2 (green) and nephrin (magenta) colocalized areas.

(F) Immunogold electron microscopy showed cell-membrane-associated binding of the anti-ILDR2 antibody in podocyte foot processes. Scale bars represent 1 μm (Figures B–F).

tTJs homeostasis is known to disrupt the equilibrium of epithelium barrier function and monolayer organization, resulting in dysplasia. In 2021, Sugawara et al. also reported that aberrant expression angulin-1/LSR implicated the epithelial barrier function due to the loss of plasma membrane contact at the tTJs point. Furthermore, in 2017, a single-cell RNA sequencing study identified ILDR2 as a podocyte-specific gene which was shown to be essential for the actin cytoskeleton in cultured podocytes.[7] Recently, the group of O'Brian has shown that ILDR2 was associated with podocin along the slit diaphragm.[8] This raised the question of where exactly ILDR2 is located in the glomeruli and what role ILDR2 plays in the podocytes. Using different methods and studying ILDR2 knockout mice, we investigated whether ILDR2 is essential for podocyte morphology and function as well as for the size selectivity of the filtration barrier.

RESULTS

Podocytes express the tricellular tight junction-associated protein ILDR2

Tricellular junctions are a universal feature of epithelial cells and contain tricellulin (MARVELD2) which is bound to at least one angulin (ILDR1, ILDR2, or LSR). In the Sampson Normal Tissue microarray dataset of the Nephroseq database (www.nephroseq.org) derived from microdissected human kidneys, *ILDR2* was enriched in the glomerular fraction in comparison to other kidney fractions (Figure 1A). Single-cell RNA sequencing of murine kidneys showed that in comparison to the other angulins, *Ildr2* was enriched within the podocyte cluster together with the podocyte-specific claudin, claudin-5 (Figure 1B). We verified these findings by quantitative reverse-transcription PCR (RT-qPCR) of isolated murine glomeruli, which showed a significantly glomerulus-enriched expression of *Ildr2* in comparison with total kidney fractions (Figure 1C).

Chromogenic single-RNA *in situ* hybridization using the RNAscope method showed the specific presence of *ILDR2* mRNA exclusively in podocytes in healthy human kidney tissue sections (Figure 1D). In a published isolated podocyte versus bulk glomerulus mass spectrometry dataset, podocyte-specificity of ILDR2 in comparison to whole glomeruli could be verified (Figure 1E). Anti-ILDR2 western blots of isolated glomeruli (purity indicated by the presence of nephrin) versus the whole kidney fraction were performed. Glomerular lysates probed with a polyclonal anti-ILDR2 antibody showed a single band of around the predicted size of 71 kDa (Figure 1F).

Immunofluorescence staining using a specific antibody against ILDR2 detected an epitope in murine and human glomeruli which produced a punctate staining pattern (Figures 2A and S1). Confocal laser scanning micrographs (C-LSM) showed that within glomeruli, ILDR2-spots colocalized with nephrin, a marker of the

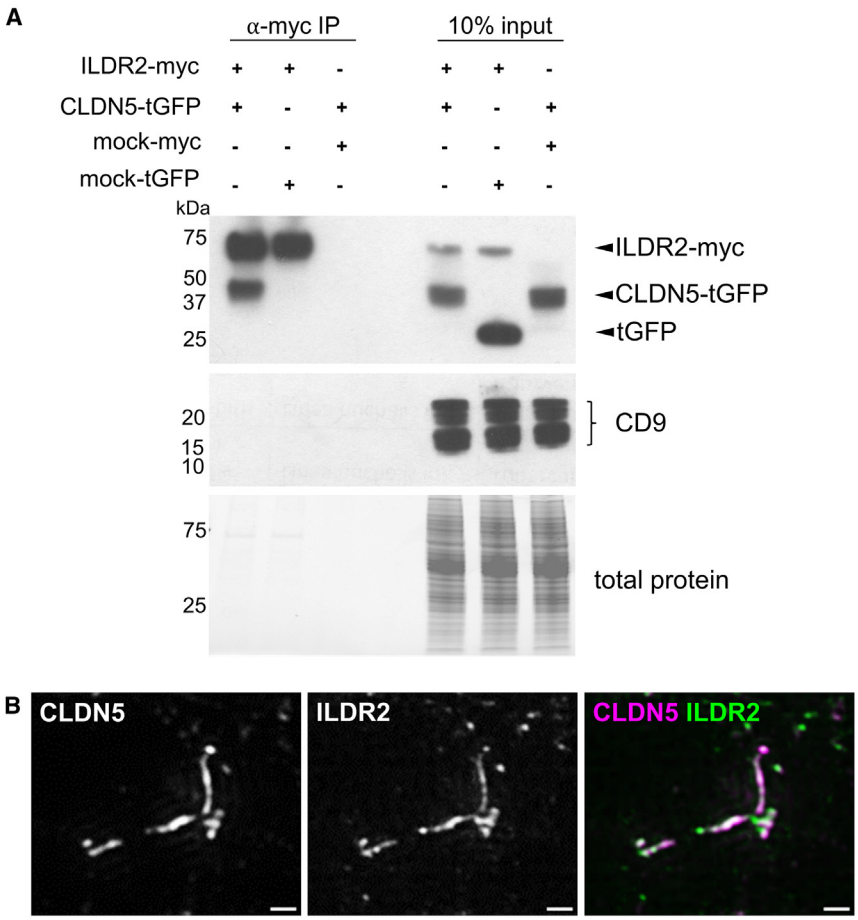

Figure 3. ILDR2 is an integral component of podocyte bi- and tricellular junctions and forms a complex with the podocyte-specific claudin-5

(A) Co-immunoprecipitation experiments of ILDR2-myc and CLDN5-GFP followed by western blot analysis with indicated antibodies. "Input" means the sample on 10% of volume used for IP. Anti-CD9 western blot served as a (non-binding) negative control.

(B) The expression of ILDR2 (green) colocalized with CLDN5 (magenta) in human nephrectomy kidney glomeruli of FFPE sections in areas of podocyte foot process effacement. Imaged by SR-SIM. Scale bars represent 500 nm.

podocyte slit diaphragm in mouse and human tissue sections (Figure 2A).

Super-resolution 3-dimensional (3D)-structured illumination microscopy (3D-SIM) revealed that ILDR2 localized at tricellular junctions as indicated by co-staining with nephrin on intersections of the nephrin-stained filtration slit (Figure 2B). Additional to this, focal ILDR2 localized to some bicellular junctions in a punctated manner. These ILDR2-positive junctions were associated within normally formed foot processes (Figure 2C). Immunogold transmission electron microscopy (TEM) validated this observation. Here we found that ILDR2 localized to the cell membrane of podocyte foot processes (Figure 2F). The corresponding controls are shown in Figure S1B. In the absence of the primary antibody, no signal was detected. For comparison, a polyclonal anti-podocin antibody was used as a positive control (Figure S1B).

Looking in embryonic mouse kidneys at E19 by 3D-SIM, ILDR2 was broadly localized to the developing filtration slits (Figure 2D). The areas where nephrin and ILDR2 colocalized were more frequent and broader compared to healthy adult sections. In areas where podocyte foot processes were broadened (effaced), ILDR2 also colocalized to the filtration slits in a linear and colocalized manner in adult mice, as demonstrated by using 3D-SIM (Figure 2E).

ILDR2 interacts with the podocyte-specific claudin-5

CLDN5 has been shown to be the podocyte-specific claudin in bicellular tight junctions which is recruited and increased during the development of podocyte foot process effacement.[11] Using co-immunoprecipitation (coIP) of HEK-293 cells that were co-transfected with ILDR2-myc and CLDN5-tGFP, we found an interaction of both proteins (Figure 3A). In double-transfected cells, Cldn5-tGFP could be detected in anti-myc pull-down eluates, whereas single-transfected cells did not show a signal. Additionally, analysis of immunofluorescence stainings by SR-SIM (Superresolution Structured Illumination Microscopy) showed that the expression of ILDR2 was colocalized with CLDN5 in human kidney glomeruli in areas of podocyte foot process effacement (Figure 3B).

ILDR2 is up-regulated in different glomerulopathies in mice and human

To find out the role of ILDR2 *in vivo*, we analyzed different murine models of glomerular disease. In mice which were treated with nephrotoxic serum to induce crescentic glomerulonephritis as well as in the desoxycorticosterone acetate (DOCA) salt/ uninephrectomy (UNX) mice, a model to mimic hypertension-induced glomerular damage, we found an up-regulation of the protein level as well as mRNA by immunofluorescent staining and *in situ* hybridization (Figures 4A–4F).

Furthermore, *Ildr2* mRNA levels were significantly up-regulated in diabetes mouse glomeruli (Figure 4I) and in 24 weeks old diabetic ob/ob mice compared to wild-type control (Figure 4J). To compare the expression of *ILDR2* between glomerulopathies and healthy individuals, we analyzed microarray data from glomeruli from kidney biopsies of patients diagnosed with diabetic nephropathy (DN), minimal change disease (MCD), focal segmental glomerulosclerosis (FSGS), and rapidly progressive glomerulonephritis (RPGN) and found a significant increase of *ILDR2* expression in the glomeruli of MCD and FSGS patients (Figure 4K).

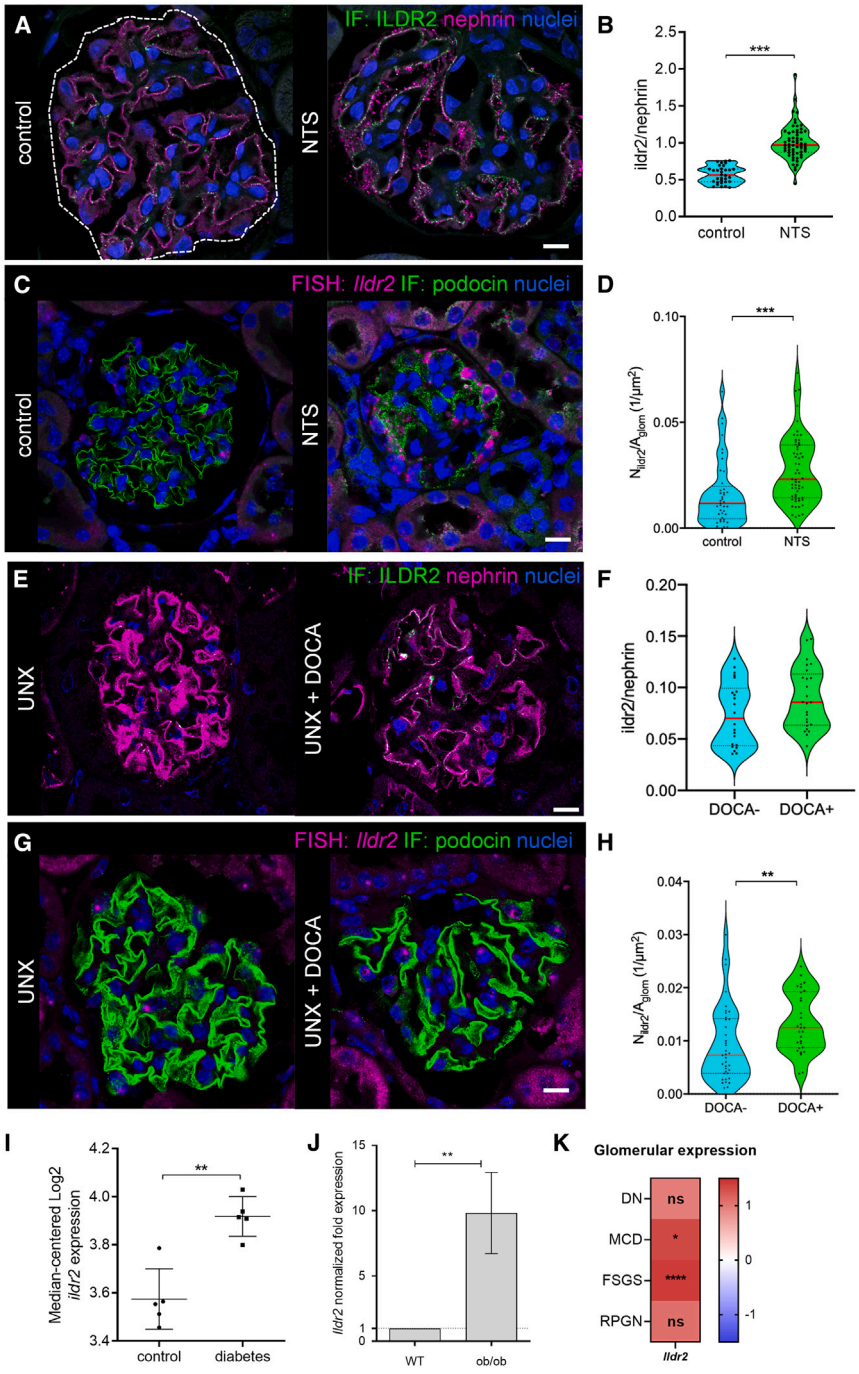

Figure 4. ILDR2 is up-regulated in DOCA-salt/UNX and NTS-treated mice as well as in different human glomerulopathies

(A–H) ILDR2 expression (shown in green) in control and NTS-treated mice (A) or uninephrectomy (UNX) and desoxycorticosterone acetate (DOCA)-salt-treated mice (E).

Nephrin (magenta) served as a podocyte-specific marker. NTS injected mice (B) and DOCA-salt treated (F) mice showed significantly increased ildr2/nephrin ratio. RNAScope of *Ildr2* (magenta) followed by quantification of ILDR2 positive spots per glomerulus area ($1/\mu m^2$) in NTS-treated mice (C and D) and DOCA-salt-treated mice (G and H) confirmed the increased expression of *Ildr2* after injury. Podocin (shown in green) served as a podocyte marker.

(I) Analysis of diabetes mouse glomeruli (Nephroseq database) substantiated increased expression on mRNA levels of *Ildr2* in diabetes mice ($n = 5$) compared to Ctrl ($n = 5$).

(J) An increase in the *Ildr2* expression was also observed in ob/ob mice ($n = 18$).

(K) mRNA expression level of microdissected glomeruli from renal biopsies of human patients suffering from diabetic nephropathy (DN; $n = 7$), minimal change disease (MCD; $n = 5$), focal segmental glomerulosclerosis (FSGS; $n = 10$) and rapidly progressive glomerulonephritis (RPGN, $n = 23$) compared with healthy living donors (LD; $n = 18$). Data are represented as log2 fold change, a q-value < 0.05 was considered as significant. Red: up-regulated to LD. Data are presented as means ± SD (I), means ± SEM (J), or violin plot (B, D, F, and H); $^{*}p < 0.05$; $^{**}p < 0.01$; $^{***}p < 0.001$; $^{****}p < 0.0001$ ns, not significant. Scale bars represent 10 μm.

Ildr2 knockout mice do not develop proteinuria or changes of podocyte foot processes

Ildr2 knockout animals (*Ildr2* KO) were generated by crossing animals with a floxed exon 1 of the *Ildr2* gene with a CMV:Cre line (Figure 5A). The Cre was removed by backcrossing to the background strain (C57BL/6J). Offspring were produced in the expected mendelian ratios and developed without obvious phenotypic changes. The efficient knockout of *Ildr2* was verified with reverse-transcription PCR (RT-PCR) and RT-qPCR which showed no significant amplicon (Figures 5B and 5C). Both western blot and immunofluorescence staining showed no binding of the anti-ILDR2 antibody in the kidneys of knockout animals (Figures 5D and S2A). TEM revealed a significant thickening of the glomerular basement membrane (GBM) in *Ildr2* KO mice (Figure 5E). However, no significant increase in podocyte foot process effacement was observed in comparison to WT mice (Figure 5E). Analysis by podocyte exact morphology measurement procedure (PEMP) showed a slightly but not significantly reduced filtration slit diaphragm density (FSD) in *Ildr2* KO mice compared to WT mice (3.98 μm^{-1} versus 4.31 μm^{-1}) (Figure 5F). Model-based glomerular morphometry showed slight glomerular hypertrophy with reduced podocyte density (Figures 5G–5I). However, animals did not show significantly elevated albuminuria in comparison to corresponding wild-type littermates (ACR (albumin-to-creatinine ratio) in μg/mg: WT: 15; KO: 42) (Figure 5J).

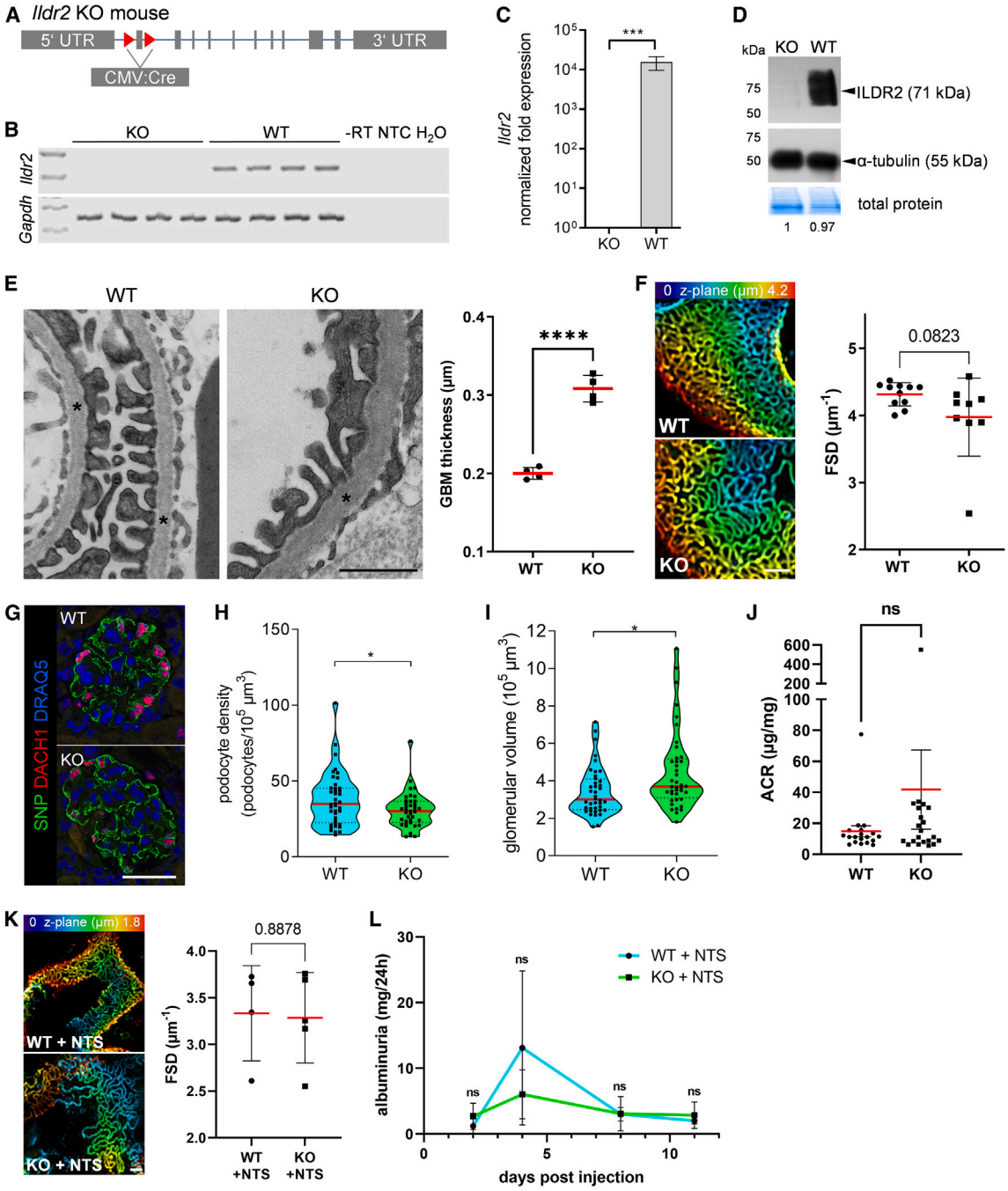

Figure 5. *Ildr2* knockout mice do not develop proteinuria but have altered podocyte morphology

(A) Schemata of *Ildr2* whole-body knockout animals by crossing animals with a floxed exon 1 of the ILDR2 gene with a CMV:Cre line.

(B) *Ildr2* KO verification by RT-PCR.

(C) *Ildr2* KO verification by RT-qPCR. Gapdh served as a reference.

(D) *Ildr2* KO verification by western blot. Alpha-tubulin and total protein served as a loading control.

(E) Transmission electron microscopy of wild-type (WT) and *Ildr2* knockout (KO) mice revealed a significantly increased glomerular basement membrane (GBM) thickness in *Ildr2* KO mice compared to WT mice (thickening indicated by asterisks; dots represent individual animals).

(F) 3D-SIM in *Ildr2* KO animals showed no significantly reduced filtration slit density (FSD) indicative for aberrant FP architecture. SIM data of 11 WT and 9 KO animals were quantified by PEMP (at 12 months of age). Kidney sections were stained for the slit diaphragm protein podocin. z axis scales of 3D-SIM were color coded as indicated.

(G) Immunofluorescence staining for DACH1 (red) and the podocyte-specific marker synaptopodin (SNP; shown in green) in *Ildr2* KO and WT mice.

(H and I) Model-based glomerular morphometry showed slight glomerular hypertrophy with reduced podocyte density.

(legend continued on next page)

After NTS (nephrotoxic serum)-induced glomerulonephritis, we also found no significant decrease of the FSD as a marker for podocyte foot process effacement and no significantly increased albuminuria in *Ildr2* KO mice compared to WT animals (Figure 5K and 5L).

Ildr2 KO mice show glomerular profibrotic alterations but no compensatory up-regulation of angulin or other tight junction proteins

To find out which other proteins are regulated by the loss of ILDR2, we performed proteomic profiling of isolated glomeruli from five independent WT and five *Ildr2* KO mice by LC-MS/MS. We detected 140 significantly up- and 155 down-regulated proteins in the *Ildr2* KO mice compared to WT ($p < 0.05$ and log2 fold change ≥ 0.3) (Figure 6A and Data S1). Proteomic data impressively showed that actin-associated proteins were significantly down-regulated in *Ildr2* KO glomeruli (Figure 6A). In contrast, extracellular matrix (ECM) proteins such as collagens and fibronectin were significantly up-regulated in *Ildr2* KO glomeruli (Figures 6B–6D). Furthermore, periodic acid-Schiff (PAS) staining demonstrated that *Ildr2* KO mice exhibited increased glomerular matrix accumulations as well as an increase in glomerulosclerosis (glomerular PAS+ area) (Figure 6E).

Interestingly, at the protein level, no increase of other angulins such as ILDR1 or LSR in the *Ildr2* KO animals was detected. Using RT-qPCR, we analyzed the mRNA levels of *Ildr1*, *Cldn1*, *Lsr*, and *Marveld2*. None of them showed significant changes due to the loss of *Ildr2* (Figure 6F). This was also confirmed by analysis of immunofluorescence stainings (Figure 6G). Furthermore, claudin-5 and the tight junction protein ZO-1 also showed no significant regulation at mRNA (Figure 6F) or protein level (Figures 6H, 6I, S2B, and S2C). Furthermore, no increased albumin uptake was detected in the renal tubules (Figure S2D).

DISCUSSION

Podocytes are important for proper blood filtration and form a specialized cell-cell junction between their interdigitating foot processes. Since the seminal paper of the Farquhar group, it has been known that this cell-cell contact contains specialized adherens and tight junction features.[1] Therefore, specific cell-cell contacts of healthy and diseased podocytes are of great importance.

As it has been already demonstrated that podocytes sporadically form tricellular junctions under healthy conditions,[2] we wanted to investigate which proteins of the tricellular tight junction complex are expressed between interdigitating podocyte foot processes. In the present study, we show that the angulin ILDR2 is localized at these tricellular junctions under healthy conditions which is in agreement with a recent publication of Higashi et al.[12] Furthermore, we identified ILDR2 at bicellular junctions of broadened foot processes by super resolution fluorescence light microscopy and immunoelectron microscopy. However, it was not possible to find out whether there is an association of ILDR2 to tTJs by using immunoelectron microscopy. This can be explained by the fact that the probability of visualizing this protein using non-volumetric electron microscopy to tricellular junctions is low. Therefore, super resolution 3D-SIM was used to identify ILDR2 at tricellular junctions. Interestingly, this localization pattern changed after the broadening of podocyte foot processes. After such an effacement, the localization was extended from tricellular to bicellular tight junctions. A similar shift was found for the podocyte-specific tight junction protein claudin-5.[11] Instead of a punctate distribution along the slit diaphragm, it changed to a linear pattern after an effacement of the podocyte foot process.[13] This is in contrast to the localization in embryonic kidneys, where ILDR2 was found only in a bicellular linear pattern. This is in line with the observation that during nephrogenesis tight junctions are the main cell-cell contact between podocytes and a shift from bicellular to tricellular junctions occurred during maturation. It could be suggested that podocyte foot process effacement might be the inverse of the developmental process.[14]

To get a deeper understanding of how ILDR2 is localized at the slit diaphragm, we performed co-immunoprecipitation. With this method, we were able to identify an interaction of ILDR2 and claudin-5, suggesting that ILDR2 is integrated within the slit diaphragm in a complex with claudin-5. This is supported by the finding of an earlier work, where ILDR2 has been pulled-down from the vicinity of the slit diaphragm by proximity-dependent *in vivo* biotinylation.[8] But it is still unclear whether ILDR2 is an integral part of this complex or not. In this work, over the binding of claudin-5, we propose a way in which ILDR2 could be integrated within this complex. To reveal whether ILDR2 was essential for the integrity of the size selectivity of the filtration barrier, we phenotyped ILDR2 whole-body knockout mice. After validation of the loss of the *Ildr2* expression in podocytes, we analyzed the urinary creatinine/albumin ratio. Surprisingly, we have not found any significant changes in podocyte foot processes. However, we have observed an increase of the glomerular size, indicating hyperfiltration with consecutive glomerular hypertrophy.

The precise function of tTJs in regulating paracellular permeability across epithelia has been a subject of investigation. In 2017, Krug demonstrated in an *in vitro* assay that tTJs facilitate up to 29% of paracellular macromolecule flux, in particularly tight epithelial cell monolayers.[13] Conversely, in cells with more permeable tight junctions, the contribution of tTJs to flux is rather minimal.

Consequently, it can be postulated that in podocytes, which experience significant paracellular flux due to glomerular filtration and, therefore, are a rather leaky epithelium, the regulatory role of tTJs in permeability may be less significant compared to tight epithelia. This is in line with Higashi et al., who

(J) Urinary albumin-creatinine ratio measurements indicated no significantly increased levels of proteinuria in *Ildr2* KO mice in comparison to WT animals (each individual dot represents one experimental animal).

(K) *Ildr2* KO mice also showed no significantly reduced filtration slit density (FSD) in comparison to WT mice after NTS-induced glomerulonephritis.

(L) Level of albuminuria in *Ildr2* WT and KO mice at day 2, 4, 8, and 11 after NTS injection. Scale bars represent 1 μm (E, F, and K) or 50 μm (G). Data are presented as means ± SD (C, F, J, K, and L) or violin plot (H and I); *$p < 0.05$; **$p < 0.01$; ****$p < 0.0001$; ns, not significant.

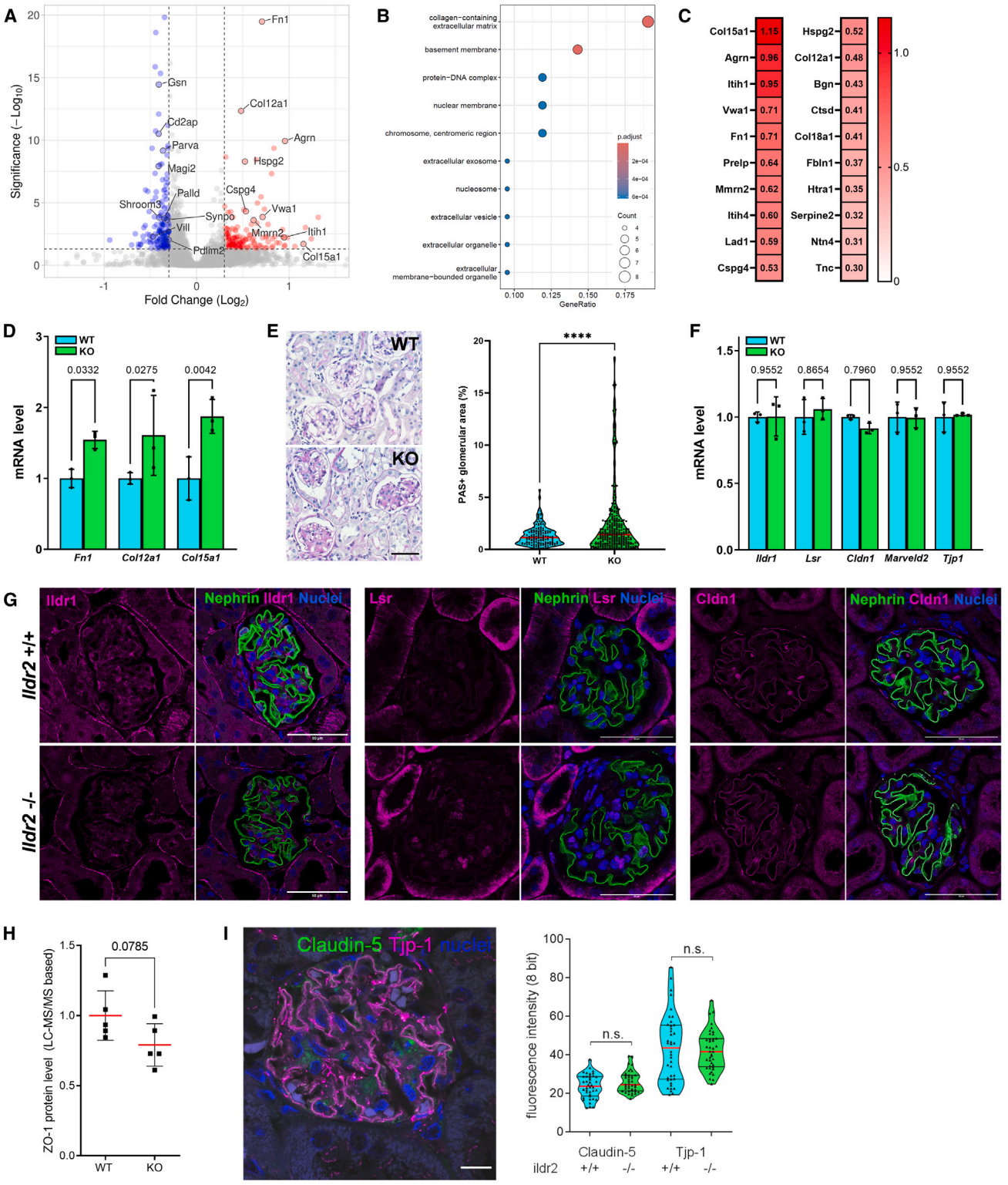

Figure 6. *Ildr2* KO glomeruli showed increased expression of extracellular matrix proteins, but no up-regulation of potentially compensatory angulin or tight junction proteins

(A) Volcano plot displaying proteins with significantly changed abundance in *Ildr2* KO glomeruliin comparison to wild-type glomeruli ($n = 5$). Blue: down-regulated compared to controls; red: up-regulated compared to controls. Given are proteins with a log2 fold-change ≥ 0.3 and p value ≤ 0.05.

(legend continued on next page)

demonstrated in 2013 that ILDR2 provided a rather weak transepithelial barrier in comparison to the other angulins when transfected in epithelial cell monolayers.[3]

Therefore, while it is recognized that tTJs can influence the passage of smaller macromolecules across epithelia, their impact on macromolecular selectivity within the glomerular filtration barrier appears to be rather limited.[15] Suggesting that depletion of ILDR2 resulted in a gross disruption of ILDR2-containing tTJs, this could be an explanation why *Ildr2* KO animals were not proteinuric, as the baseline flux of macromolecules like albumin across tTJs appears to be negligible under steady-state conditions.

Proteomic profiling of isolated glomeruli of *Ildr2* KO animals revealed that the *Ildr2* KO had a significant impact on different signaling pathways. We have identified the up-regulation of several extracellular matrix proteins indicating a pro-fibrotic glomerular phenotype. This was confirmed by PAS staining in *Ildr2* knockout animals, which exhibited increased glomerular matrix.

The hypothesis suggests that alterations in the tricellular junctions of podocytes may not affect the filtration barrier's selectivity but might influence signaling between podocytes and mesangial cells, leading to extracellular matrix deposition. Interestingly, matrix accumulation in KO mice treated with NTS was significantly reduced compared to the control animals. Since ILDR2 can modulate immune signaling and is involved in alternative splicing,[16] further studies should explore this aspect in more detail.

Since no change of the size selectivity of the filtration barrier occurred in *Ildr2* KO animals, we wanted to find out whether one of the other known angulin proteins was locally up-regulated to rescue the ILDR2 loss in podocytes. However, we have not found an up-regulation of ILDR1 or LSR. Besides these candidates, we have not detected other tight-junction-associated proteins that could be responsible for a rescue of the loss of ILDR2.

In summary, our results show that ILDR2 is an important component of the glomerular filtration barrier, with increased expression and localization observed in various glomerulopathies. While loss of ILDR2 does not change podocyte foot process morphology, it affects podocyte number and matrix expression, suggesting to be a counterplayer of profibrotic events during glomerulopathies.

Limitations of the study

The study focuses primarily on animal models, so the direct applicability of these results to patients remains uncertain and further research is needed. In addition, an *in vitro* overexpression model was used to study the interaction between ILDR2 and CLDN5. However, this approach does not allow any conclusion as to whether the observed interaction takes place directly in living cells or whether other proteins are essential for its relevance.

RESOURCE AVAILABILITY

Lead contact

Further information and requests for resources and reagents should be directed to and will be fulfilled by the lead contact, Nicole Endlich (nicole.endlich@uni-greifswald.de).

Materials availability

This study did not generate new unique reagents.

Data and code availability

- All data supporting the findings of this study are available within the paper and its supplemental information.
- The mass spectrometry proteomics data are available in supplementary data files (Data S1) and have been deposited to the ProteomeXchange Consortium via the PRIDE partner repository and are publicly available as of the date of publication. Accession number is listed in the key resources table.
- Any additional information required to reanalyze the data reported in this paper is available from the lead contact upon request.

ACKNOWLEDGMENTS

This work was supported by a start-up grant of the Research Network Molecular Medicine and by a grant of the Gerhard-Domagk Masterclass of the University Medicine Greifswald to Florian Siegerist and by grants of the Federal Ministry of Education and Research (BMBF, STOP-FSGS grant 01GM1518B and 01GM2202B; Sys_CARE grant 01ZX1908B and 01ZX2208B) to N.E. and U.V. M.L. is supported by BMBF, grant 01GM2202A; STOP-FSGS and BMBF grant 01EK2105D, UPTAKE. We thank all participating centers of the European Renal cDNA Bank-Kroener-Fresenius Biopsy Bank (ERCB-KFB) and their patients for their cooperation. Active members at the time of the study are listed in ref. (Martini et al. JASN 2014, Vol 25, No 11, 2559–2572). P.S. was supported by a scholarship from the Gerhard-Domagk program of the University Medicine Greifswald. We thank Victor Puelles (University Medical Center Hamburg-Eppendorf) for model-based glomerular morphometry. This work was generously supported by the Südmeyer Stiftung für Nieren- und Gefäßforschung and the Dr. Gerhard Büchtemann fund, Hamburg, Germany. The funders had no role in study design, data collection and analysis, decision to publish, or preparation of the manuscript. We would like to thank Heimke von Osten for the human kidney biopsies. The graphical abstract has been created using images from BioRender.com.

(B) Top 10 GO (Gene Ontology) CC (cellular components) clusters, which were significantly up-regulated in *Ildr2* KO glomeruli.
(C) Significantly up-regulated extracellular matrix proteins in *Ildr2* KO mice. Data are represented as log2 fold change, a p value <0.05 was considered as significant. (D) Renal mRNA expression of *Fn1*, *Col12a1* and *Col15a1* in *Ildr2* WT and *Ildr2* KO mice (n = 3).
(E) Histologic evaluation of glomerular damage pattern employing Periodic acid-Schiff staining (PAS). At 12 months of age, expansion of the mesangial compartment was detectable. Assessment of glomerulosclerosis (glomerular PAS+ area) confirmed glomerular damage (each dot represents one individual glomerulus (WT: n = 144; KO: n = 299); seven WT and eight KO animals were analyzed).
(F) The mRNA expression of *Ildr1*, *Lsr*, *Cldn1*, *Marveld2*, and *Tjp1* was not significantly regulated in *Ildr2* −/− mice (n = 4). RT-qPCR experiments were normalized to wild-type mice (WT), *Gapdh* served as a reference. ns, not significant.
(G) Immunofluorescence staining for ILDR1, LSR and CLDN1 (magenta) and the podocyte-specific marker nephrin (shown in green) in *Ildr2* KO (*Ildr2* −/−) and WT mice (*Ildr2* +/+).
(H) LC-MS/MS based relative protein level of ZO-1 (TJP1) in isolated glomeruli from *Ildr2* KO and *Ildr2* WT mice (n = 5).
(I) Fluorescence intensity measurement of immunofluorescence stained glomeruli with specific antibodies against claudin-5 and Tjp1 (ZO-1). Data are presented as means ± SD (D, G, and I) or violin plot (E and J); p value is indicated; ****p < 0.0001; n.s., not significant. Scale bars represent 50 μm (E and G) and 10 μm (I).

AUTHOR CONTRIBUTIONS

The study was designed by F.S. and N.E.; F.S. and C.W. contributed to the cell culture experiments; biopsies were handled and analyzed by F.S., P.S., J.E.C.S., and M.L.; LC-MS/MS was performed by E.H. and U.V.; animal experiments were performed by F.S., C.W., S.R.-W., M.C.B., C.C., and C.E.C.; western blots and IP were performed and quantified by F.S., C.W., and F.K..; V.D. performed PEMP; all other experiments were performed by F.S.; experimental data were analyzed by F.S., F.K., P.S., E.H., and S.S.; M.N. analyzed urine; F.S., F.K., and N.E. wrote the main manuscript text; F.S. and F.K. prepared figures. All authors reviewed the manuscript.

DECLARATION OF INTERESTS

The authors declare no competing interests.

STAR★METHODS

Detailed methods are provided in the online version of this paper and include the following:

- KEY RESOURCES TABLE
- EXPERIMENTAL MODEL AND STUDY PARTICIPANT DETAILS
  - Generation of *Ildr2* KO mice
  - DOCA-salt induced hypertension
  - Mouse model of nephrotoxic serum–induced GN
  - BTBR ob/ob mouse model of type 2 diabetes
- METHOD DETAILS
  - Immunofluorescence staining
  - Single-mRNA *in situ* hybridization (RNAscope) and combined fluorescence *in situ* hybridization and immunofluorescence
  - Co-immunoprecipitation and western blot
  - RNA extraction, cDNA synthesis and qRT-PCR
  - Histology and transmission electron microscopy
  - Liquid chromatography-mass spectrometry (LC-MS/MS)
  - Morphometry
  - Microarrays on human kidney biopsies
  - Microscopy
- QUANTIFICATION AND STATISTICAL ANALYSIS

SUPPLEMENTAL INFORMATION

Supplemental information can be found online at https://doi.org/10.1016/j.isci.2024.111329.

Received: May 23, 2024
Revised: August 5, 2024
Accepted: November 4, 2024
Published: November 7, 2024

REFERENCES

1. Fukasawa, H., Bornheimer, S., Kudlicka, K., and Farquhar, M.G. (2009). Slit diaphragms contain tight junction proteins. J. Am. Soc. Nephrol. *20*, 1491–1503. https://doi.org/10.1681/ASN.2008101117.
2. Ichimura, K., Miyazaki, N., Sadayama, S., Murata, K., Koike, M., Nakamura, K.-I., Ohta, K., and Sakai, T. (2015). Three-dimensional architecture of podocytes revealed by block-face scanning electron microscopy. Sci. Rep. *5*, 8993. https://doi.org/10.1038/srep08993.
3. Higashi, T., Tokuda, S., Kitajiri, S., Masuda, S., Nakamura, H., Oda, Y., and Furuse, M. (2013). Analysis of the 'angulin' proteins LSR, ILDR1 and ILDR2–tricellulin recruitment, epithelial barrier function and implication in deafness pathogenesis. J. Cell Sci. *126*, 966–977. https://doi.org/10.1242/jcs.116442.
4. Oda, Y., Otani, T., Ikenouchi, J., and Furuse, M. (2014). Tricellulin regulates junctional tension of epithelial cells at tricellular contacts through Cdc42. J. Cell Sci. *127*, 4201–4212. https://doi.org/10.1242/jcs.150607.
5. Sugawara, T., Furuse, K., Otani, T., Wakayama, T., and Furuse, M. (2021). Angulin-1 seals tricellular contacts independently of tricellulin and claudins. J. Cell Biol. *220*, e202005062. https://doi.org/10.1083/jcb.202005062.
6. Cho, Y., Haraguchi, D., Shigetomi, K., Matsuzawa, K., Uchida, S., and Ikenouchi, J. (2022). Tricellulin secures the epithelial barrier at tricellular junctions by interacting with actomyosin. J. Cell Biol. *221*, e202009037. https://doi.org/10.1083/jcb.202009037.
7. Lu, Y., Ye, Y., Bao, W., Yang, Q., Wang, J., Liu, Z., and Shi, S. (2017). Genome-wide identification of genes essential for podocyte cytoskeletons based on single-cell RNA sequencing. Kidney Int. *92*, 1119–1129. https://doi.org/10.1016/j.kint.2017.04.022.
8. Gerlach, G.F., Imseis, Z.H., Cooper, S.L., Santos, A.N., and O'Brien, L.L. (2023). Mapping of the podocin proximity-dependent proteome reveals novel components of the kidney podocyte foot process. Front. Cell Dev. Biol. *11*, 1195037. https://doi.org/10.3389/fcell.2023.1195037.
9. Ransick, A., Lindström, N.O., Liu, J., Zhu, Q., Guo, J.-J., Alvarado, G.F., Kim, A.D., Black, H.G., Kim, J., and McMahon, A.P. (2019). Single-Cell Profiling Reveals Sex, Lineage, and Regional Diversity in the Mouse Kidney. Dev. Cell *51*, 399–413.e7. https://doi.org/10.1016/j.devcel.2019.10.005.
10. Rinschen, M.M., Gödel, M., Grahammer, F., Zschiedrich, S., Helmstädter, M., Kretz, O., Zarei, M., Braun, D.A., Dittrich, S., Pahmeyer, C., et al. (2018). A Multi-layered Quantitative In Vivo Expression Atlas of the Podocyte Unravels Kidney Disease Candidate Genes. Cell Rep. *23*, 2495–2508. https://doi.org/10.1016/j.celrep.2018.04.059.
11. Tesch, F., Siegerist, F., Hay, E., Artelt, N., Daniel, C., Amann, K., Zimmermann, U., Kavvadas, P., Grisk, O., Chadjichristos, C., et al. (2021). Super-resolved local recruitment of CLDN5 to filtration slits implicates a direct relationship with podocyte foot process effacement. J. Cell Mol. Med. *25*, 7631–7641. https://doi.org/10.1111/jcmm.16519.
12. Higashi, A.Y., Saito, A.C., Higashi, T., Furuse, K., Furuse, M., Chiba, H., and Kazama, J.J. (2024). Bicellular Localization of Tricellular Junctional Protein Angulin-3/ILDR2 Allows Detection of Podocyte Injury. Am. J. Pathol. *194*, 673–683. https://doi.org/10.1016/j.ajpath.2024.01.008.
13. Krug, S.M. (2017). Contribution of the tricellular tight junction to paracellular permeability in leaky and tight epithelia. Ann. N. Y. Acad. Sci. *1397*, 219–230. https://doi.org/10.1111/nyas.13379.
14. Ichimura, K., Kakuta, S., Kawasaki, Y., Miyaki, T., Nonami, T., Miyazaki, N., Nakao, T., Enomoto, S., Arai, S., Koike, M., et al. (2017). Morphological process of podocyte development revealed by block-face scanning electron microscopy. J. Cell Sci. *130*, 132–142. https://doi.org/10.1242/jcs.187815.
15. Krug, S.M., Amasheh, S., Richter, J.F., Milatz, S., Günzel, D., Westphal, J.K., Huber, O., Schulzke, J.D., and Fromm, M. (2009). Tricellulin forms a barrier to macromolecules in tricellular tight junctions without affecting ion permeability. Mol. Biol. Cell *20*, 3713–3724. https://doi.org/10.1091/mbc.e09-01-0080.
16. Liu, Y., Nie, H., Liu, C., Zhai, X., Sang, Q., Wang, Y., Shi, D., Wang, L., and Xu, Z. (2017). Angulin proteins ILDR1 and ILDR2 regulate alternative pre-mRNA splicing through binding to splicing factors TRA2A, TRA2B, or SRSF1. Sci. Rep. *7*, 7466. https://doi.org/10.1038/s41598-017-07530-z.
17. Millings, E.J., De Rosa, M.C., Fleet, S., Watanabe, K., Rausch, R., Egli, D., Li, G., Leduc, C.A., Zhang, Y., Fischer, S.G., et al. (2018). ILDR2 has a negligible role in hepatic steatosis. PLoS One *13*, e0197548. https://doi.org/10.1371/journal.pone.0197548.
18. Bankhead, P., Loughrey, M.B., Fernández, J.A., Dombrowski, Y., McArt, D.G., Dunne, P.D., McQuaid, S., Gray, R.T., Murray, L.J., Coleman, H.G., et al. (2017). QuPath: Open source software for digital pathology image analysis. Sci. Rep. *7*, 16878. https://doi.org/10.1038/s41598-017-17204-5.

19. Schordan, S., Grisk, O., Schordan, E., Miehe, B., Rumpel, E., Endlich, K., Giebel, J., and Endlich, N. (2013). OPN deficiency results in severe glomerulosclerosis in uninephrectomized mice. Am. J. Physiol. Ren. Physiol. *304*, F1458–F1470. https://doi.org/10.1152/ajprenal.00615.2012.

20. Artelt, N., Ludwig, T.A., Rogge, H., Kavvadas, P., Siegerist, F., Blumenthal, A., van den Brandt, J., Otey, C.A., Bang, M.-L., Amann, K., et al. (2018). The Role of Palladin in Podocytes. J. Am. Soc. Nephrol. *29*, 1662–1678. https://doi.org/10.1681/ASN.2017091039.

21. Schindelin, J., Arganda-Carreras, I., Frise, E., Kaynig, V., Longair, M., Pietzsch, T., Preibisch, S., Rueden, C., Saalfeld, S., Schmid, B., et al. (2012). Fiji: an open-source platform for biological-image analysis. Nat. Methods *9*, 676–682. https://doi.org/10.1038/nmeth.2019.

22. Richardson, K.C., Jarett, L., and Finke, E.H. (1960). Embedding in epoxy resins for ultrathin sectioning in electron microscopy. Stain Technol. *35*, 313–323. https://doi.org/10.3109/10520296009114754.

23. Blankenburg, S., Hentschker, C., Nagel, A., Hildebrandt, P., Michalik, S., Dittmar, D., Surmann, K., and Völker, U. (2019). Improving Proteome Coverage for Small Sample Amounts: An Advanced Method for Proteomics Approaches with Low Bacterial Cell Numbers. Proteomics *19*, e1900192. https://doi.org/10.1002/pmic.201900192.

24. Kliewe, F., Siegerist, F., Hammer, E., Al-Hasani, J., Amling, T.R.J., Hollemann, J.Z.E., Schindler, M., Drenic, V., Simm, S., Amann, K., et al. (2024). Zyxin is important for the stability and function of podocytes, especially during mechanical stretch. Commun. Biol. *7*, 446. https://doi.org/10.1038/s42003-024-06125-5.

25. Artelt, N., Siegerist, F., Ritter, A.M., Grisk, O., Schlüter, R., Endlich, K., and Endlich, N. (2018). Comparative Analysis of Podocyte Foot Process Morphology in Three Species by 3D Super-Resolution Microscopy. Front. Med. *5*, 292. https://doi.org/10.3389/fmed.2018.00292.

26. Siegerist, F., Ribback, S., Dombrowski, F., Amann, K., Zimmermann, U., Endlich, K., and Endlich, N. (2017). Structured illumination microscopy and automatized image processing as a rapid diagnostic tool for podocyte effacement. Sci. Rep. *7*, 11473. https://doi.org/10.1038/s41598-017-11553-x.

27. Cohen, C.D., Frach, K., Schlöndorff, D., and Kretzler, M. (2002). Quantitative gene expression analysis in renal biopsies: a novel protocol for a high-throughput multicenter application. Kidney Int. *61*, 133–140. https://doi.org/10.1046/j.1523-1755.2002.00113.x.

28. Martini, S., Nair, V., Keller, B.J., Eichinger, F., Hawkins, J.J., Randolph, A., Böger, C.A., Gadegbeku, C.A., Fox, C.S., Cohen, C.D., et al. (2014). Integrative biology identifies shared transcriptional networks in CKD. J. Am. Soc. Nephrol. *25*, 2559–2572. https://doi.org/10.1681/ASN.2013080906.

29. Tusher, V.G., Tibshirani, R., and Chu, G. (2001). Significance analysis of microarrays applied to the ionizing radiation response. Proc. Natl. Acad. Sci. USA *98*, 5116–5121. https://doi.org/10.1073/pnas.091062498.

STAR★METHODS

KEY RESOURCES TABLE

REAGENT or RESOURCE	SOURCE	IDENTIFIER
Antibodies		
Anti-ILDR2	Mikio Furuse[3]	N/A
Anti-ILDR2	Thermo Fisher Scientific	Cat# HPA012815
Anti-Podocin	IBL	Cat# 29040; RRID: AB_10683302
Anti-Nephrin	Progen	Cat# GP-N2; RRID: AB_2904121
Anti-CLDN5	BiCellScientific	Cat# 00-205
Anti-CLDN5	Invitrogen	Cat# 35-2500
Anti-Synaptopodin	Progen	Cat# 61094; RRID: AB_2909601
Anti-Dach1	Sigma-Aldrich	Cat# HPA012672; RRID: AB_1847466
Anti-ILDR1	BiCellScientific	Cat# 00-302
Anti-Lsr	Invitrogen	Cat# PA5-52412; RRID: AB_2643590
Anti-CLDN1	BiCellScientific	Cat# 00-201
Anti-Tjp1	Invitrogen	Cat# 61-7300
Anti-ATP1A1	Developmental Studies Hybridoma Bank	Cat# AB_528092
Anti-Albumin	Bio-Techne GmbH	Cat# NBP1-32458; RRID: AB_10003946
Anti-CD9	GeneTex	Cat# GTX19761; RRID: AB_423722
Anti-tGFP	Origene	Cat# TA150041; RRID: AB_2622256
Biological samples		
Kidney FFPE tissues from mice	University Medicine Greifswald, Germany	N/A
Kidney FFPE tissues from human	University Medicine Greifswald, Germany	N/A
Critical commercial assays		
iTaq Universal SYBR Green Supermix	Bio-Rad	Cat# 1725124
QuantiTect Reverse Transcription Kit	Qiagen	Cat# 205311
RNAscope Brown 2.5 Kit	ACDbio	Cat# 322370
Deposited data		
Mass spectrometry proteomics data	This paper	PRIDE: PXD056696
Experimental models: Cell lines		
HEK-293	Cytion (CLS)	Cat# 300192
Experimental models: Organisms/strains		
Ildr2-floxed mice with B6.C-Tg(CMV-cre) 1Cgn/J background	Millings et al.[17]	N/A
BTBR ob/ob mice	The Jackson Laboratory	stock number: 004824
Oligonucleotides		
Primers for quantitative Real-time PCR, see Table S1	Thermo Fisher	N/A
Recombinant DNA		
Plasmid: ILDR2-myc	Origene	Cat#: MR224366
Plasmid: CLDN5-tGFP	This paper	N/A
Plasmid: pCMV6-AC-GFP	Origene	Cat#: PS100010
Plasmid: pCMV6-Entry	Origene	Cat#: PS100001
Software and algorithms		
Graphpad Prism	Graphpad	https://www.graphpad.com/scientific-software/prism/
ImageJ	NIH	https://imagej.nih.gov/ij/
QuPath v0.5.1	Bankhead, P. et al.[18]	https://qupath.github.io/

EXPERIMENTAL MODEL AND STUDY PARTICIPANT DETAILS

Generation of *Ildr2* KO mice

The *Ildr2*-floxd line was generated as described by Millings et al.[17] Whole body *Ildr2* KO mice were generated by crossing Ildr2-floxed mice with B6.C-Tg(CMV-cre)1Cgn/J (JAX:006054). Mice were housed at room temperature in a 12-hr light/12hr-dark vivarium, with *ad libitum* access standard water. The Cre was removed by backcrossing to the background strain (C57BL/6J). KO and WT animals were obtained by cross-breeding heterozygous animals. Experiments were performed with 6-24-month-old male and female mice. All studies were carried out in strict accordance with regulations in Germany regarding the use of laboratory animals.

DOCA-salt induced hypertension

Induction of glomerular hypertension by uninephrectomy (UNX) and desoxycorticosterone acetate (DOCA) salt treatment has been described previously.[19]

Mouse model of nephrotoxic serum–induced GN

Induction of NTS-induced glomerulonephritis has been described previously.[11,20]

BTBR ob/ob mouse model of type 2 diabetes

Mice derived from the strain BTBR (Black and Tan BRachyury) served as model for T2DM with BTBR WT mice as control and leptin-deficient BTBR ob/ob mice as diabetic animals. Heterozygous BTBR ob+/− mice (BTBR.Cg-Lepob/WiscJ, stock number: 004824; The Jackson Laboratory (Sacramento, CA, USA)) were used for breeding. All animal experimental procedures were approved by the local ethics committee at the University Hospital Regensburg (No.55.2-2532-2-1259).

METHOD DETAILS

Immunofluorescence staining

For immunofluorescence of Ildr2 two polyclonal antibodies were used: 1.: An ILDR2 rabbit anti-mouse antiserum was a kind gift by Mikio Furuse.[3] Polyclonal antibodies were affinity-purified using the western-blot method with the immunization peptide. Fresh-frozen wildtype mouse kidneys were embedded in OCT (Sakura) and sectioned at 10 μm using a rotational cryomicrotome (HM500; Leica Microsystems, Wetzlar, Germany) and collected on super frost slides. Sections were air dried and fixed with 1:1 ethanol-acetone for 10 min at room temperature. Slides were washed in PBS, blocked, and primary antibodies incubated o/n at 4°C. Primary antibodies were detected using Alexa Fluor 488 conjugated goat anti-rabbit $F(ab)_2$ fragments and Cy3 conjugated donkey anti-guinea pig full IgG antibodies. Nuclei were counterstained with DAPI and mounted in Mowiol for microscopy (Roth, Karlsruhe, Germany). 2.: Affinity purified rabbit anti ILDR2 antibody (Thermo Fisher Scientific, Waltham, MA, U.S.A) diluted 1:150 in blocking solution was applied on 4 μm FFPE (formaldehyde-fixed paraffin-embedded) sections of mouse tissue after heat-mediated epitope retrieval in citrate buffer pH 9. For the detection of the primary antibody, the same protocol was used as for the cryosections.

Single-mRNA *in situ* hybridization (RNAscope) and combined fluorescence *in situ* hybridization and immunofluorescence

In situ histochemistry was performed using the RNAscope Kits 2.5 Brown or Red with human and murine *ILDR2* exon 1-3, *PPIB* (positive control) and *dapB* (negative control) probes synthesized by ACDbio. Single chromogenic RNAscope was performed according to the manufacturer's instructions with the following conditions: Heat mediated antigen retrieval for 15 min, and Proteinase Plus digestion for 30 min. hybridization of primary probe for 2 h at 40°C, AMP5 30 min at RT. The suitability of every FFPE block for RNAscope was evaluated using the PPIB positive control probe. Blocks with a *PPIB* score of 2 and higher went into further *ILDR2* testing.

For combined fluorescence *in situ* hybridization and immunofluorescence, we used the RNAscope Manual 2.5 Kit Red with AP and FastRed detection with the following modifications: After FastRed incubation, sections were washed in tap water and collected in 1x PBS. After blocking with 1% normal goat serum, 1% BSA, 1% FBS and 0.1% cold fish gelatin in 1x PBS, a pre-incubated mixture of affinity purified polyclonal rabbit anti podocin antibodies (IBL) 1:150 and Alexa Fluor 488 conjugated site-specific dual monoclonal alpaca anti rabbit nano secondaries (single domain antibodies, VHHs, Chromotek) 1:1000 in blocking solution was applied to the sections at 4°C overnight. After 5 washes in 1x PBS and nuclear counterstain with DAPI, sections were mounted in Mowiol and imaged. For semi-automated analysis of the ILDR2 expression, we established a FIJI macro that after manual selection of the podocin$^+$ outlines of the glomerular tuft, segments, binarizes, and counts the *ILDR2*$^+$ spots using the Particle Analyzer function in FIJI.[21] Output values were: glomerular tuft area, ILDR2 particle number, mean and total area.

Co-immunoprecipitation and western blot

HEK-293 cells were cultured for 3 days and transfected with the respective myc or tGFP plasmid using jetPEI (Polyplus-transfection, Illkirch, France). 48h post-transfection cells were scraped in ice cold PBS. Cells were washed twice in PBS and lysed in Pierce™ IP Lysis Buffer (25 mM Tris-HCl pH 7.4, 150 mM NaCl, 1% NP-40, 1 mM EDTA, 5% glycerol) (Thermo Fisher Scientific) containing 1x Halt Protease and Phosphatase Inhibitor Cocktail (Thermo Fisher Scientific) for 20 min on ice. After removing debris by centrifugation

for 20 min at 10,000 xg, cell lysates were incubated for 1.5h at room temperature with anti-myc-Trap Magnetic Beads (ChromoTek GmbH, Planegg-Martinsried, Germany). After two washing steps (10 mM Tris/Cl pH 7.5, 150 mM NaCl, 0.5 mM EDTA) beads were resuspended in 2 × SDS loading buffer (final concentrations: 64 mM Tris-HCl, 2% SDS, 10% glycerol, 0.1% bromophenol blue, 6.5% 2-mercaptoethanol, pH 6.8) and boiled for 5 min at 95°C. Lysates were separated using a 4–20% Mini-PROTEAN® TGX™ Gel, (Bio-Rad Laboratories, Munich, Germany) and transferred to a nitrocellulose membrane using a Trans-Blot® Turbo™ Transfer System (Bio-Rad Laboratories) for 10 min at 2 A. Membranes were immersed for 1 h in blocking buffer (10 mM Tris, 100 mM NaCl, 5% non-fat dry milk, 0.2% Tween-20, pH 7.5) and incubated overnight at 4°C in TBS-Tween (0.5%) with the following antibodies: anti-ILDR2 (1:1000), anti-CLDN5 (1:1000), anti-CD9 (1:1000) and anti-tGFP (1:10000) for IP-WB. Blots were incubated for 1 h at RT with HRP–conjugated secondary antibody anti-mouse (SA00001-1, Proteintech Group) or anti-rabbit (SA00001-2, Proteintech Group) and developed using Clarity™ Western ECL Blotting Substrate (Bio-Rad Laboratories) and finally exposed to X-ray films (Fujifilm Super RX, FUJIFILM, Tokyo, Japan).

RNA extraction, cDNA synthesis and qRT-PCR

Samples were processed in Tri-Reagent (Sigma-Aldrich) according to manufacturer's instructions. For cDNA synthesis, 1 μg of the isolated total RNA was transcribed using the QuantiTect Reverse Transcription Kit (Qiagen, Hilden, Germany). The quantitative real-time PCR (qRT-PCR) analysis was performed on a QuantStudio™ 5 Real-Time PCR System (Thermo Fisher Scientific) using the iTaq Universal SYBR Green Supermix (Bio-Rad) with Gapdh as reference gene. Relative quantifications of the mRNA levels were done by the efficiency corrected calculation model by Pfaffl and are shown with standard deviations (SD) or standard error of the mean (SEM) from at least three biological replicates. Used primers can be viewed in Table S1.

Histology and transmission electron microscopy

For routine histology, tissue was fixed in 4% paraformaldehyde pH 7.4 at RT o/n and embedded in paraffin after an ascending ethanol series. Sections were cut at 2-4 μm and collected on super frost slides (Marienfeld, Lauda-Königshofen, Germany).

For transmission electron microscopy, apical cortex blocks were trimmed to 1x1 mm and fixed in 4% glutaraldehyde in 1x PBS pH 7.4 for 2 days at RT. The tissue was embedded in epoxy resin. Semi- (500 nm) and ultrathin (70 nm) sections were cut using a Leica Ultracut UCT and collected on glass slides and copper grids, respectively. Semithin sections were stained according to Richardson,[22] and ultrathin sections were contrasted with lead-citrate. The glomerular morphology of four *Ildr2* wild-type and four *Ildr2* knockout mice was evaluated. The analysis and measurement of the GBM were conducted at different positions in various capillary loops.

Liquid chromatography-mass spectrometry (LC-MS/MS)

Proteins were extracted from isolated murine glomeruli of five independent bioreplicates from *Ildr2* WT and KO mice by heating the samples for 5 min at 95°C in 20 mM Hepes buffer containing 4 % SDS. Protein containing supernatant was collected by centrifugation (16.000 x g, 60 min, 4°C) and nucleic acid degraded enzymatically with universal nuclease (0.125 U/μg protein, (Pierce/Thermo, Rockford, IL, U.S.A.). Protein concentration was determined by BCA assay (Pierce/Thermo). Four μg protein were reduced by 2.5 mM dithiothreitol for 1 h at 60°C and alkylated with 10 mM iodoacetic acid for 30 min at 37°C in the dark before subsequent protein purification and proteolytic digestion according to a modified SP3 protocol.[23] Peptides were separated by LC (Ultimate 3000, Thermo Electron, Bremen, Germany) before data-independent acquisition of MS data on an Exploris 480 mass spectrometer (Thermo Electron). MS data were analyzed via the DirectDIA algorithm implemented in Spectronaut (v14, Biognosys, Zurich, Switzerland) using Uniprot database (v.2021-02) limited to Mus musculus (n=17063). Carbamidomethylation at cysteine was set as static modification, oxidation at methionine and protein N-terminal acetylation were defined as variable modifications, and up to two missed cleavages were allowed. Proteins were only considered for further analyses, if two or more unique+razor peptides were identified and quantified per protein. Further data analysis was performed as reported earlier.[24] Detailed description of data acquisition and search parameters are provided in Table S2.

Morphometry

Podocyte foot processes width in transmission electron micrographs were quantified by counting the number of filtration slits/glomerular capillary circumferences in FIJI.[21] Processing, staining, imaging, and quantification were performed with minor modifications as described before.[25,26] In brief, 4 μm sections were directly mounted, blocked, and incubated with rabbit anti-podocin 1:150 (IBL International, Germany) and mouse anti-integrin α3 conjugated with Alexa Fluor 647 1:500 (Santa Cruz Biotechnology, Dallas, USA) and anti-rabbit Alexa Fluor 488 conjugated IgG 1:600 (ChromoTek, Germany) secondary antibody. Widefield and 3D-SIM images were acquired on an N-SIM super-resolution microscope (Nikon, Japan). To account for the 3-dimensional architecture of the filtration slit, 19 z-plane images were obtained to generate a maximum intensity projection (MIP) image. 3D-SIM images were reconstructed using NIS-Elements AR software (Nikon, Japan). Digital post-processing, profile plotting, and podocyte exact morphology measurement procedure (PEMP) was performed using FIJI combined with a custom-built macro described before.[26] First, in a whole slide image, glomeruli were segmented with an AI, and glomeruli with section artifacts or poor staining quality are excluded. The algorithm determined the total filtration slit length (FSL) based on podocin staining and the total podocyte foot process area based on integrin α3 staining (A). Filtration slit diaphragm density (FSD) was then calculated from the ratio of FSL over A.

Microarrays on human kidney biopsies

Human renal biopsy specimens and Affymetrix microarray expression data were procured within the framework of the European Renal cDNA Bank - Kröner-Fresenius Biopsy Bank. Biopsies were obtained from patients after informed consent and with approval of the local ethics committees. Following renal biopsy, the tissue was transferred to RNase inhibitor and microdissected into glomeruli and tubulointerstitium. Total RNA was isolated from microdissected glomeruli, reverse transcribed, and linearly amplified according to a protocol previously reported.[27,28]

Previously generated microarray data from microdissected human glomeruli sourced from individuals with kidney disease and healthy donors were used (Affymetrix HGU133Plus2.0: GEO accession number: GSE47185 (H7-Glom: Affymetrix HGU133Plus2.0)). Pre-transplantation kidney biopsies from living donors were used as control (GEO accession number: GSE37463 (H7-Glom: Affymetrix HGU133Plus2.0)). CEL file normalization was performed with the Robust Multichip Average method using RMAExpress (version 1.20) and the human Entrez-Gene custom CDF annotation from Brain Array (version 25). To identify differentially expressed genes, the SAM (Significance Analysis of Microarrays) method was applied using SAM function in Multiple Experiment Viewer (TiGR MeV, Version 4.9).[29] A q-value below 5% was considered to be statistically significant. Analysis included gene expression profiles from patients with diabetic nephropathy (DN; n=7), minimal change disease (MCD; n=5), focal segmental glomerulosclerosis (FSGS; n=10) and rapidly progressive glomerulonephritis (RPGN, n=23) as well as controls (living donors, n=18).

Microscopy

Confocal laser scanning microscopy images were captured by a Leica TCS-SP5 system (Leica Microsystems) with a 63x 1.4 NA oil immersion objective or an Olympus FV3000 (Olympus, Tokyo, Japan) with 20x/40x/60x oil immersion objectives and the following laser wavelengths: 405nm, 488 nm, 561 nm, and 640 nm (Olympus FV3000 CellSense software). For super-resolution imaging, a 3D-structured illumination microscope (Zeiss Elyra PS.1 system, Carl Zeiss Microsystems, and Nikon N-SIM-E) was used as described before.[26] Whole-slide images of PAS-stained sections were acquired on a Nikon ECLIPSE Ti2-E. Files were imported and processed with QuPath (v0.5.1).[18]

QUANTIFICATION AND STATISTICAL ANALYSIS

The GraphPad Prism 9 software was used for statistical analysis of experimental data and preparation of graphs. Scatter plots indicate individual units used for statistical testing (samples, cells or replicates), as specified in the respective figure legends. Data are given as means ± SD or ± SEM, analyzed by unpaired t test with repeated measurements (n).

For multiple groups statistical analyses were done by ANOVA followed by a Benjamini-Hochberg post-hoc test. Statistical significance was defined as $p < 0.05$ and significance levels are indicated as * $p < 0.05$, ** $p < 0.01$, *** $p < 0.001$, **** $p < 0.0001$ or non-significant (ns). The number of independent experiments and analyzed units are stated in the figure legends.